Article

Application of Integrated Geological and Geophysical Surveys on the Exploration of Chalcedony Deposits: A Case Study on Nanhong Agate in Liangshan, China

Shengping Gong [1,2], Keqiang Zhao [1,2,*], Mingming Wang [3], Shengwu Yan [4,5], Yong Li [1,2] and Jianzhou Yang [1,2,*]

1   Institute of Geophysical and Geochemical Exploration, Chinese Academy of Geological Sciences, Langfang 065000, China; gshengping@mail.cgs.gov.cn (S.G.)
2   Key Laboratory of Geophysical Electromagnetic Probing Technologies of Ministry of Natural Resources, Langfang 065000, China
3   Institute of Regional Geological Survey of Hebei Province, Langfang 065000, China
4   Sichuan Institute of Comprehensive Geological Survey, Chengdu 610081, China
5   Evaluation and Utilization of Strategic Rare Metals and Rare Earth Resources Key Laboratory of Sichuan Province, Chengdu 610081, China
*   Correspondence: zkeqiang@mail.cgs.gov.cn (K.Z.); yjianzhou@mail.cgs.gov.cn (J.Y.)

Abstract: Nanhong agate, esteemed for its vivid color and natural shine, is experiencing a scarcity in supply despite its high demand. The primary deposits of agate, typically found near the surface, have not been extensively explored due to the predominance of traditional manual excavation methods. This research examined the Nanhong agate deposits in the Zhaojue–Meigu region of Liangshan, China, employing the integration of geological and geophysical surveys. Field geological surveys allowed us to outline the general areas where agate is found. Following this, using magnetic surveys, vertical electrical sounding, and controlled-source audio magnetotellurics, agate deposits were located within the conglomerate layer of the second member of the Feixianguan Formation from the Lower Triassic period at depths of less than 100 m. Our results identify mineralized layers, Xuanwei Formation mudstone, and the underlying bedrock, thus supporting the creation of a mineral prediction map. This research provides essential insights and guidance for agate exploration and the development of associated mineral resources.

Keywords: agate deposits; Liangshan; geological survey; vertical electrical sounding; controlled-source audiomagnetotelluric method

1. Introduction

The jadeite mineral group is highly esteemed in the gemstone market due to its variety of colors and textures [1,2]. Among these variants, Nanhong agate stands out for its rich crimson hue and exquisite texture, commanding significant popularity among consumers. Among these, Nanhong agate is particularly notable for its deep crimson color and fine texture, making it highly popular among buyers. Nanhong refers to a specific type of red agate found in the southwestern part of China. Notably, the Nanhong agate deposits in the Zhaojue–Meigu area of Liangshan, Sichuan Province, China, are renowned for their pristine condition [3,4]. The formation of Nanhong agate is linked with the creation of the nearby Emeishan basalt during the late Permian period. Volcanic activities during this period enabled the mineralization of agate through the percolation of silica-rich hydrothermal fluids containing metal ions, which imparted the distinctive coloration. Further geological processes, such as weathering and erosion, shaped these agate minerals, leading to the abundant presence of Nanhong agate pebbles. These pebbles were then deposited within the sedimentary layers of the Xuanwei and Feixianguan groups in the Zhaojue–Meigu area, forming secondary ore deposits [5,6].

Despite the high economic value of Nanhong agate, exploration in the region largely depends on outdated manual excavation methods. These methods are inherently inefficient and largely fortuitous, underscoring the necessity for more scientifically rigorous and efficient exploration techniques. Although geophysical methods offer considerable benefits for mineral exploration [7–12], their use in jadeite mineral investigations has been relatively limited. Therefore, this study seeks to assess the efficacy of integrated geophysical methods in the exploration of Nanhong agate deposits. We conducted a detailed and systematic exploration of Nanhong agate deposits in the Liangshan area, building on field geological surveys and employing a suite of geophysical techniques, including magnetic surveying, vertical electrical sounding (VES), and the controlled-source audiomagnetotelluric (CSAMT) method.

Geological investigations revealed that the conglomerate bed of the Lower Triassic Feixianguan Formation harbors Nanhong agate deposits, buried at depths of less than 100 m. Through the application of geophysical methods, we delineated ore-bearing layers, identified the low-resistivity mudstone of the Xuanwei Formation, and mapped the underlying bedrock. This comprehensive characterization facilitated the development of a mineral prediction map, offering insights into the precise distribution of agate-bearing layers. Our study establishes a scientific foundation for the accurate localization and evaluation of Nanhong agate deposits while also introducing innovative methodologies for jadeite mineral exploration. We anticipate that our findings will contribute to the sustainable development and utilization of Nanhong agate resources, thereby advancing exploration efforts in the domain of chalcedony mineral deposits.

2. Geological Background

The study area, located in the southwestern part of Sichuan Province, China, is part of the Emeishan large igneous province. The exposed strata primarily include the Emeishan Basalt Formation of the Upper Permian, the Xuanwei Formation, and the Feixianguan Formation of the Lower Triassic (Figures 1 and 2).
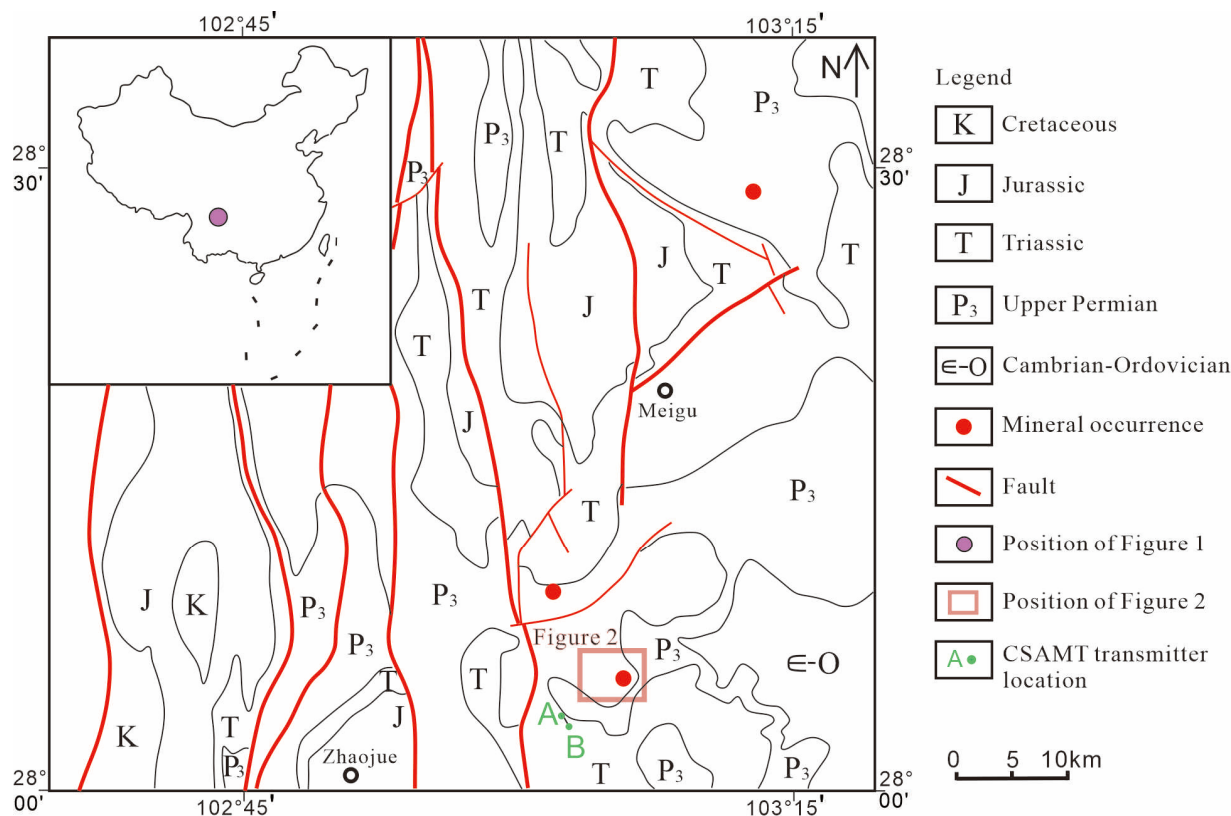

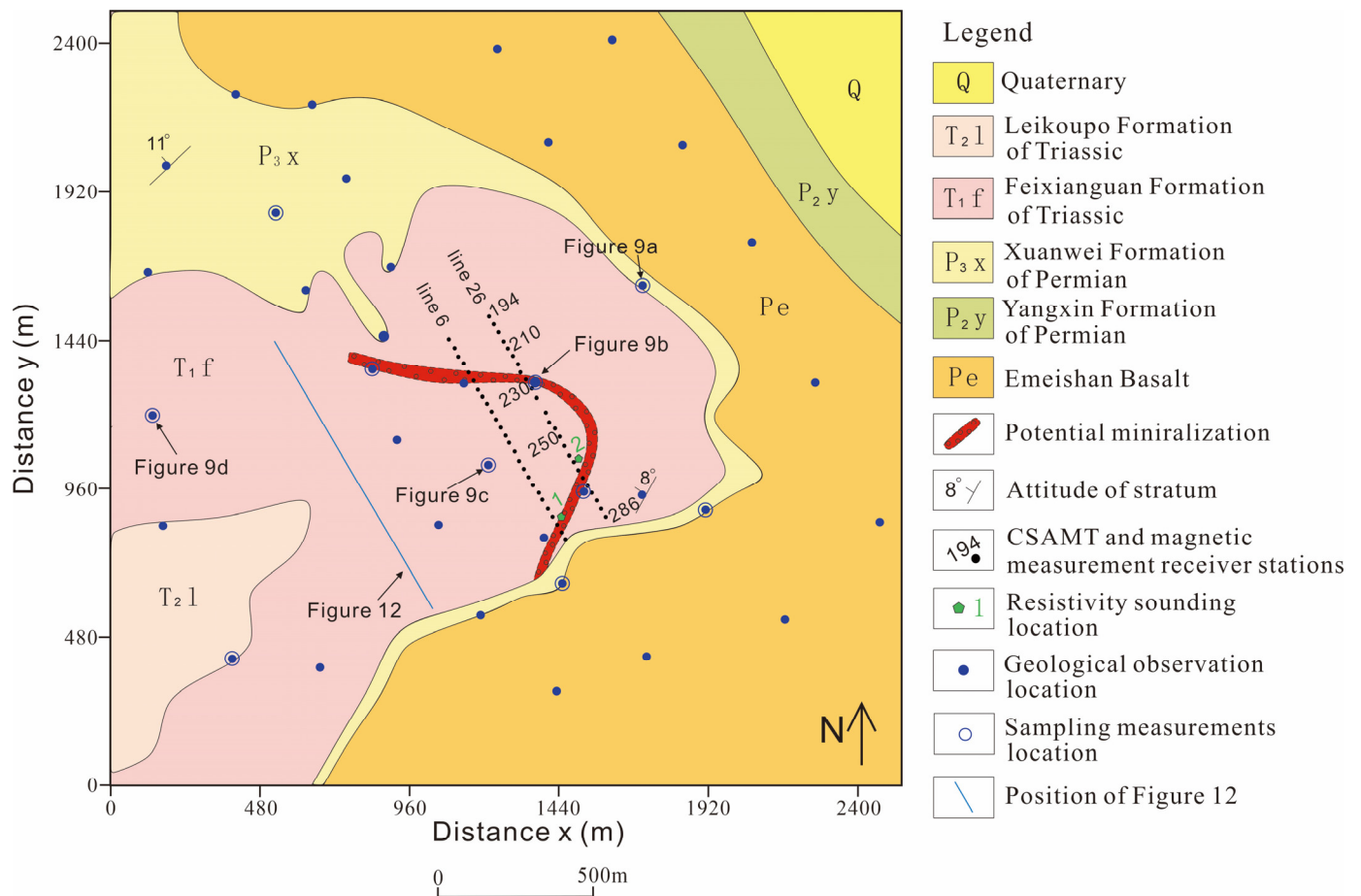**Figure 1.** Simplified geological map of the study area.

Figure 2. Geological map of the exploration area with measurement points (locations of geological and geophysical surveys are shown in the figure).

The Emeishan Basalt Formation comprises dense, mottled basalts often interbedded with volcanic breccias or tuffaceous sandstones. It nonconformably comes into contact with the underlying Yangxin Formation of the Upper Permian, with a thickness exceeding 200 m [5].

The Xuanwei Formation (P_3x) is characterized by fine-grained sandstone and iron-bearing claystone, with purple-red claystone at the base, coal-bearing mudstone in the middle, and grayish-green lithic sandstone at the top. It lies nonconformably over the Emeishan Basalt Formation, exhibiting significant weathering and sedimentary discontinuities [13].

The Feixianguan Formation (T_1f) is widespread in the study area, featuring consistent lithology with a thickness ranging from 193 to 259 m [5]. It primarily consists of purple-red gravelly feldspathic quartz sandstone and sandy shale, with gravel layers dominated by siliceous rocks and occasional agate gravel. Based on its lithological attributes, the Feixianguan Formation can be categorized into three members. The first member is characterized by thin-bedded, purple-red, medium-grained lithic sandstone alternating with purple-red thin-bedded mudstone. The second member consists of a medium–thick-bedded conglomerate displaying rhythmic layers of conglomeratic sandstone with numerous agate pebbles embedded within. Notably, sandstone layers exhibit distinct parallel bedding, tabular cross-bedding, and wedge-shaped cross-bedding. The third member comprises purple-red sandstone and fine sandstone interbedded with purple-red siltstone and mudstone. Of economic significance, agate deposits are predominantly situated within the second member of the Feixianguan Formation (Figure 3).
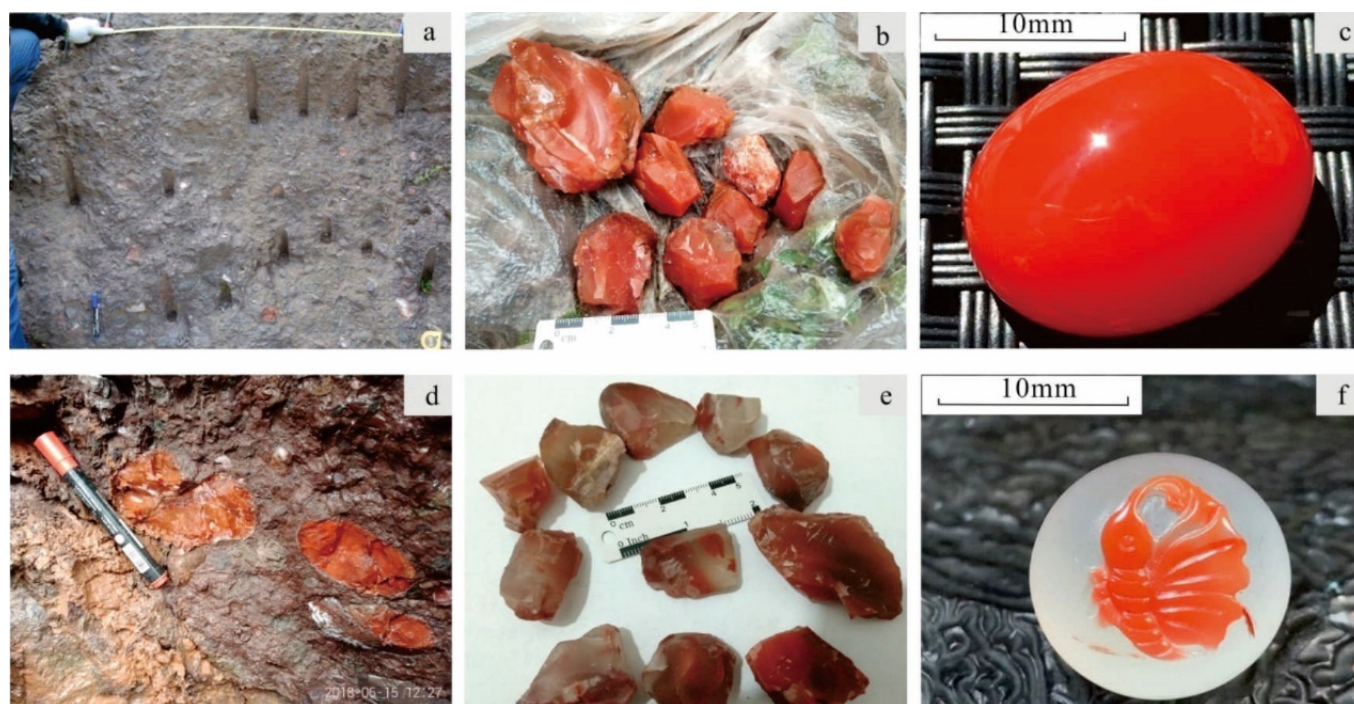
Figure 3. Field and processed photos of agate minerals. (**a**) Agate conglomerate of the Feixianguan Formation; (**b**) raw cherry-red agate; (**c**) processed cherry-red agate; (**d**) fresh cherry-red agate with red jasper outcrop; (**e**) ice-drift red agate; (**f**) processed ice-drift red agate.

3. Methodology

3.1. Field Geological Survey

A field geological survey was conducted to elucidate the ore-bearing strata of Nanhong agate, examine the sedimentary environment within the exploration area, and characterize corresponding lithological features. This process facilitated the rapid delineation of the exploration area. Initially, the survey involved the preliminary identification of lithological types, material compositions, sedimentary characteristics, ore-bearing potential, contact relationships, and spatiotemporal distribution variations in sedimentary rock layers. Concurrently, lithostratigraphic sequences were established, and an analysis of their depositional facies and environments was conducted. Furthermore, stratigraphic profiles were measured to discern ore-bearing structures and lithological assemblages. The prospecting and delineation of ore-bearing rock layers, coupled with the identification of specific lithological layers associated with mineralization, were undertaken. Additionally, structural features and mineralization alterations related to ore formation were studied. This phase of research aimed to provide a foundational understanding for subsequent geophysical exploration efforts. The locations of geological observations and sampling are marked in Figure 2.

3.2. Physical Property Measurements

The measurement of the physical properties of rock specimens contributes to the evaluation of feasibility and the interpretation of geophysical surveys [14]. Representative rock samples were collected from the field superficially and from the artificial mining cave, and they were subjected to laboratory-based measurements of magnetic and electrical resistivity properties. The samples of gravel with conglomerate agate and sandstone were taken from the cave, while the samples of basalt were collected superficially. The sampling was carried out at a few locations of the geological observation (Figure 2). Prior to laboratory measurements, samples were processed under water-cooled conditions using a tabletop drill and a cutting machine to produce cylindrical specimens with standardized dimensions: approximately 22 mm in height and 25 mm in diameter. Magnetic susceptibility parameters

were determined using a British MS2 magnetic susceptibility meter [15], with a resolution of 2×10^{-6} SI units. Subsequently, following saturation in water for over 24 hours, electrical resistivity parameters were measured using an RP-1 rock and mineral electrical conductivity meter [16]. A total of 128 samples, comprising sandstone, conglomerate, and basalt, were collected for physical property measurements.

3.3. Geophysical Exploration

High-resolution magnetic survey is a geophysical method that involves observing and analyzing magnetic anomalies caused by differences in the magnetic properties of rocks and ores, thereby studying the geological structures and distribution patterns of mineral resources. It investigates the distortion of the geomagnetic field caused by the superposition of magnetic fields generated by magnetic bodies on Earth [17–21]. In this study, the presence of highly magnetic basalt may cause overlapping magnetic anomalies with conglomerates, which should be distinguished during the analysis. Total field measurements were conducted using a PMG-2 proton magnetometer manufactured by the Czech company Satisgeo [22], with diurnal variations corrected to obtain magnetic anomalies. Prior to operation, on-site performance checks were carried out for all instruments used in the study, including accuracy calculations and inter-instrument consistency tests, to ensure proper functioning and accuracy requirements.

We generally use the induced polarization method or electrical and electromagnetic methods for electrically conductive mineral exploration [9,10,23–25], and sometimes, depending on the properties of the targeted mineral and associated host rock types, we could use ground penetrating radars (GPRs) [26] and other geophysical methods. The chalcedony ore does not have polarization characteristics and has its own properties, so we used magnetic, VES, and CSAMT methods. CSAMT is an electromagnetic sounding technique that uses finite-length grounded electric dipoles as current transmitting sources to simultaneously measure electrical and magnetic fields at a certain distance from the source dipole [11,12,27,28]. It effectively delineates subsurface electrical resistivity or conductivity information, although its resolution for near-surface is relatively limited. In this study, an equatorial dipole setup was used for scalar measurements, simultaneously observing the horizontal components of the electric field (E_x) parallel to the source and the magnetic field (H_y) orthogonal to the source. Subsequently, impedance resistivity was calculated using the electric field amplitude (E_x) and magnetic field amplitude (H_y), and the impedance phase was calculated using the electric field phase and the magnetic field phase. The resistivity parameters were inverted using a joint inversion of impedance resistivity and impedance phase. The study employed the GDP32$^{\text{II}}$ multifunctional electrical method workstation manufactured by Zonge [29], USA. The transmitter electrodes were set at AB = 800 m, receiver–transmitter separation was set at 6 ca. km (Figure 1), measuring receivers had a separation of MN = 40 m, and the frequency range was set at 8–8192 Hz, with a detection depth of 440 m.

With respect to resistivity sounding, VES employs a symmetric four-electrode configuration, in which four electrodes—A, M, N, and B(A and B as current electrodes and M and N as potential electrodes)—are arranged in a straight line and are systematically spread about the midpoint O of MN [30]. An increase in the distance between transmitting electrodes A and B is used to achieve deeper probing of the electrical characteristics of subsurface geological structures. The range of AB spans from 3 to 800 m, with a probing depth of 160 m. This method provides high resolutions for near-surface geological units but is less effective in detecting deep geological bodies and is time consuming.

Two CSAMT profiles (line 6 and line 26) were deployed along the agate mineralization zone, as shown in Figure 2. The line spacing was 200 m, and the profile direction was 150°. Finally, two resistivity sounding points were established on the profiles: VES 1 on line 6 and VES 2 on line 26. A symmetric four-electrode setup was used, with AB ranges of 3–700 m for VES 1 and 3–800 m for VES 2.

4. Results and Discussion

4.1. Geological Measurements

The Nanhong agate deposit, classified as a chalcedony-type deposit, can be further differentiated into volcanic and sedimentary types based on its genesis [31,32]. Field surveys reveal predominantly stratiform ore bodies within sedimentary rocks, manifested as conglomerates and pebbly sandstones, which are indicative of a secondary sedimentary origin. These deposits predominantly stem from the early Permian agate layers of the Emeishan basalt group. Over time, these layers underwent weathering, erosion, and redeposition, resulting in the current agate layers observed within the Feixianguan Formation. This formation, which can be subdivided into three members, is predominantly characterized by purple-red conglomerates, sandstones, and siltstones interspersed with agate-bearing conglomerate layers.

Notably, the agate-bearing layers are primarily confined to the second member of the Feixianguan Formation. These layers are characterized by medium-grained volcanic conglomerates with minor occurrences of sandstone and mudstone. These hard layers, marked by siliceous cementation, host an agate ore grade of 2–3%, predominantly featuring cherry-red agate, with some occurrences of floating ice-red and white agate. These distinctive agate-bearing layers, harder than the adjacent strata and with a gravel content ranging from 60% to 70%, are predominantly composed of volcanic rocks. The grain size within these conglomerates varies from 3 mm to 10 cm, with a predominant range of 1–5 cm. Geological observations indicate gentle dip angles of 5°–15° in the agate layers, suggesting ease of mining.

Further investigations highlight that both the roof and floor of these agate deposits pertain to the second member (T_1f^2) of the Feixianguan Formation within the Triassic system. The roof is characterized by purple-red thin–medium-grained quartz siltstones exhibiting horizontal bedding, whereas the floor is dominated by purple-red medium-grained feldspathic quartz sandstones with parallel bedding and minor cross-bedding. Specialized geological surveys pinpoint the sedimentary environment of this formation as a tidal deltaic phase and delta plain subphase. The hard-cemented agate-bearing conglomerates at the base correspond to the main river channel microfacies, while the upper sandy mudstone-cemented conglomerates are indicative of debris flow microfacies. Sandstone layers with parallel bedding represent inter-channel microfacies. The unique sedimentary environments associated with the agate layers, combined with distinct lithological features, offer valuable insights for narrowing down the exploration area, as illustrated in Figures 2 and 4.
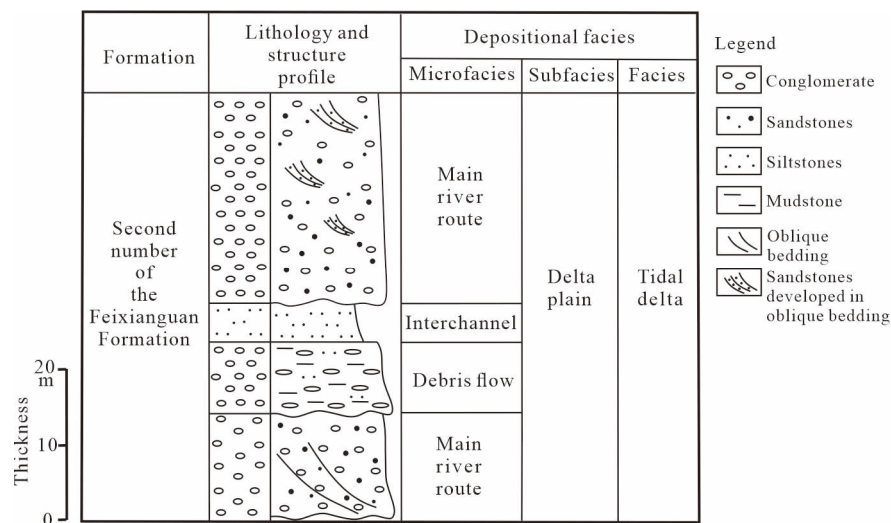

Figure 4. A representative sedimentary sequence of the second member of the Feixianguan Formation (results of this field geological survey).

4.2. Physical Property Measurements

Table 1 presents the physical property measurements of conglomerate, sandstone, and basalt samples collected from the exploration area. However, the mudstone samples in this area proved to be extremely fragile, making it impossible for us to produce suitable specimens for analysis. So, it is not shown in Table 1. The measurements reveal distinct characteristics among the rock types. Conglomerates exhibit medium to high resistivity and significant magnetic variations, generally displaying strong magnetism. In contrast, sandstones have lower resistivity and are essentially non-magnetic. Basalts demonstrate high resistivity with pronounced magnetism. Mudstones, due to their water content, exhibit low resistivity. Importantly, conglomerates containing agate display higher magnetism compared to sandstones. Thus, targeting conglomerate layers with medium characteristics can effectively guide the exploration and prospecting of agate deposits.

Table 1. Statistical parameters of rock physical properties in the study area.

Name	Samples	Susceptibility (K) ($\times 10^{-6}$ SI)			Resistivity (ρ) ($\Omega \cdot$m)		
		Min	Max	Mean	Min	Max	Mean
Gravel (with conglomerate and agate)	31	5059.74	18,432.87	9715.50	286.10	510.31	382.80
Sandstone	57	165.49	543.18	304.54	37.95	308.79	141.66
Basalt	40	18,493.18	78,893.85	52,644.5	957.62	2964.69	1892.01

4.3. Integrated Geophysical and Geological Section Measurements

CSAMT data were processed using the smooth-model inversion software SCSINV [33]. The RMS errors for the various measurement points ranged from 1.1 to 2.3.

Figure 5 illustrates the integrated profile of the line 6 geological and geophysical survey, sequentially presenting magnetic survey results, CSAMT data, and geological profile measurements. The topography displays notable undulations. Within the profile's central segment, magnetic anomalies remain steady, with elevated anomalies at both ends of the profile. The positions at the end of the profile indicate the presence of basalt according to the geological assessment.

The CSAMT method results delineate a 440-meter-deep section into three distinct electrical layers: a high-resistivity near-surface layer, a subsequent low-resistivity layer, and a bedrock layer characterized by high resistivity. Geological interpretations align with these electrical findings, identifying the high-resistivity layer at 30–80 m as sandstone from the Feixianguan Formation, the low-resistivity layer as mudstone from the Xuanwei Formation, and the bedrock as basalt. Notably, the sandstone of the Feixianguan Formation houses agate layers, with agate minerals discovered near mountain peaks and basalt exposures at the position of the end of the profile. The slightly higher magnetic anomalies at the position of the beginning of the profile likely indicate gravel associated with agate mineralization. However, not all moderate anomalies correspond to the agate layers. Deep-seated magnetic minerals can significantly impact surface magnetic survey results. As previously mentioned, the magnetic anomaly at the end of the profile is indicative of basalt. Consequently, vertical electrical sounding was conducted near the point 278 of line 6 to refine the depth characterization of the ore-bearing layer within the Feixianguan Formation.

Figure 6 illustrates the composite profile of the 26-line survey, which shares similarities with the 6-line results. High values of magnetic anomalies are observed at both ends of the profile. The CSAMT measurements revealed the electrical characteristics of the section, and vertical electrical sounding was carried out near the point 262 of line 26. Geological profiles also indicate the presence of agate minerals near mountain peaks and at the position at the beginning of the profile.
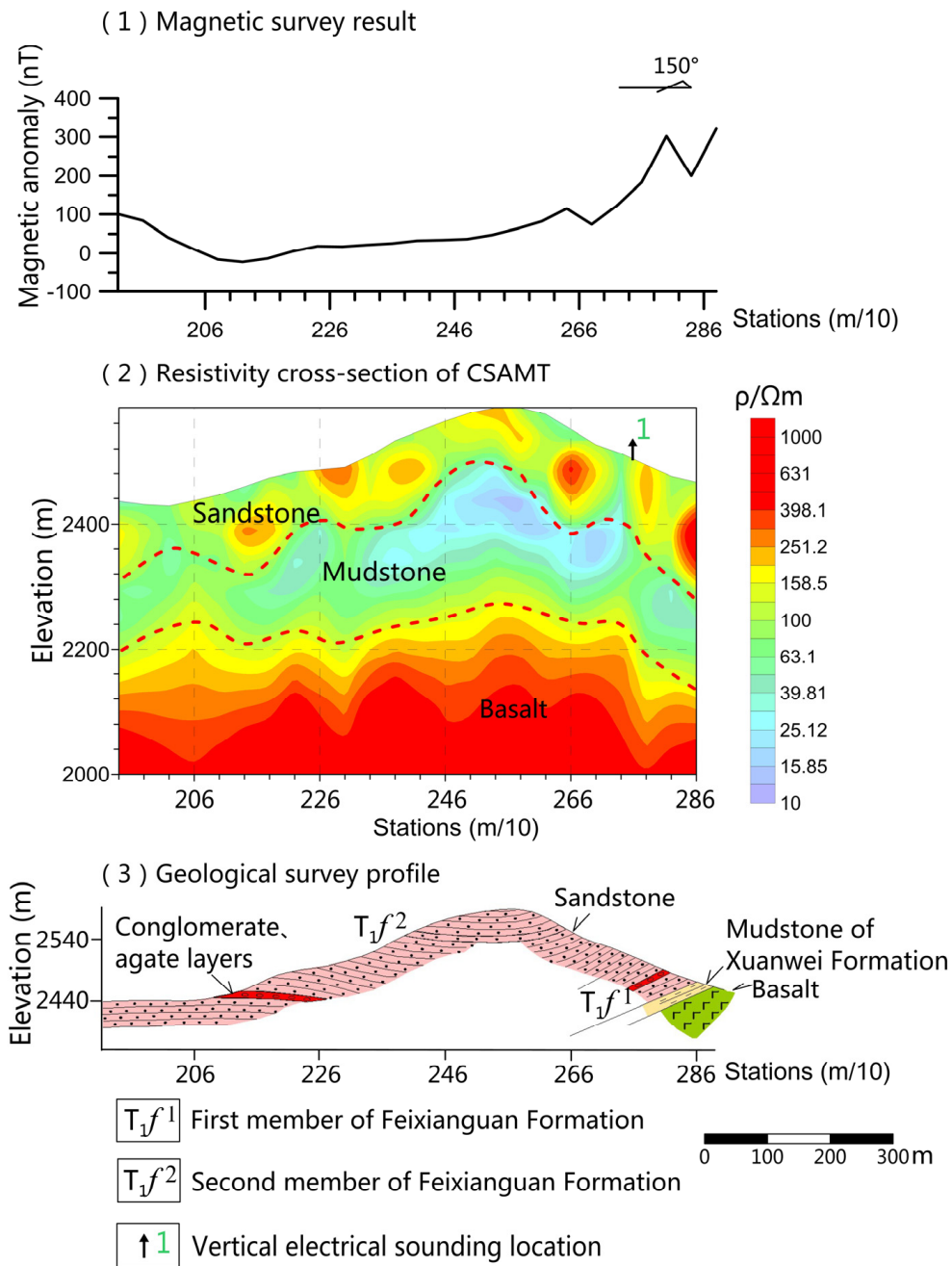
Figure 5. Geological–geophysical composite profile along the exploration line 6.

Figures 7 and 8 show the CSAMT depth soundings at various frequencies for points 206 on line 6 and 226 on line 26, respectively. This area has relatively low resistivity, with apparent resistivity values near 100 Ωm. The signal transitions to the near-field around 100 Hz. One key feature of CSAMT is that as the frequency decreases, the depth of detection increases. The curves (Figure 7) imply a simplified three-layer electrical structure from shallow to deeper depths. Formulas to convert electric and magnetic fields with respect to impedance resistivity and phases are described in [34].
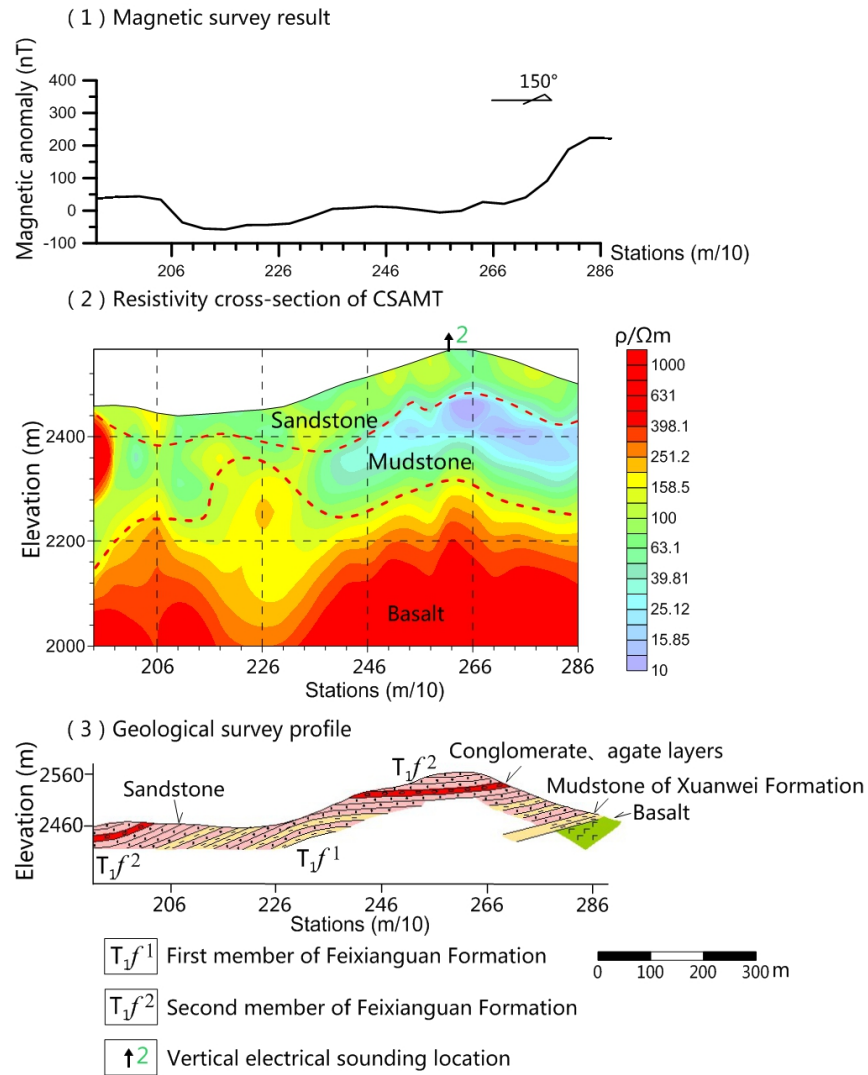
(1) Magnetic survey result

(2) Resistivity cross-section of CSAMT

(3) Geological survey profile

T_1f^1	First member of Feixianguan Formation
T_1f^2	Second member of Feixianguan Formation
↑2	Vertical electrical sounding location

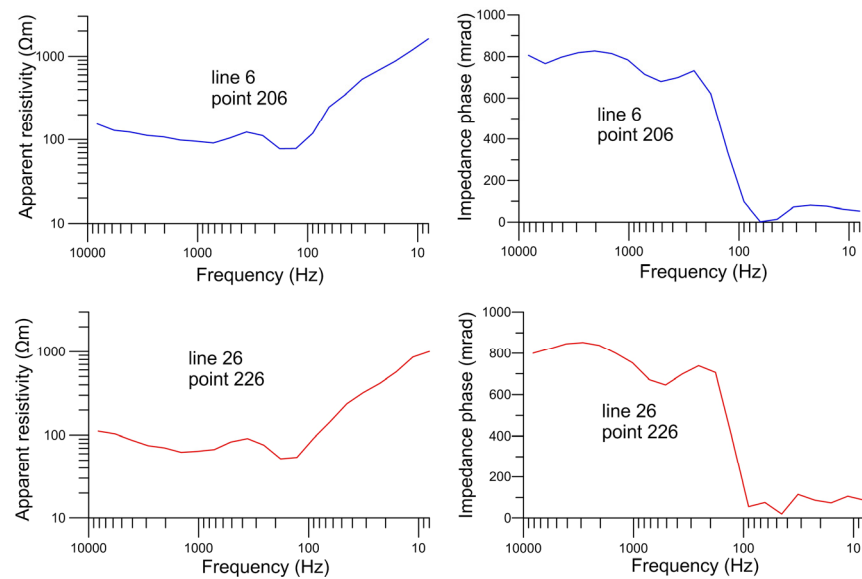**Figure 6.** Geological–geophysical composite profile along exploration line 26.

Figure 7. Controlled-source audiomagnetotelluric measurement with apparent resistivity (**left**) and impedance phase (**right**) curves.
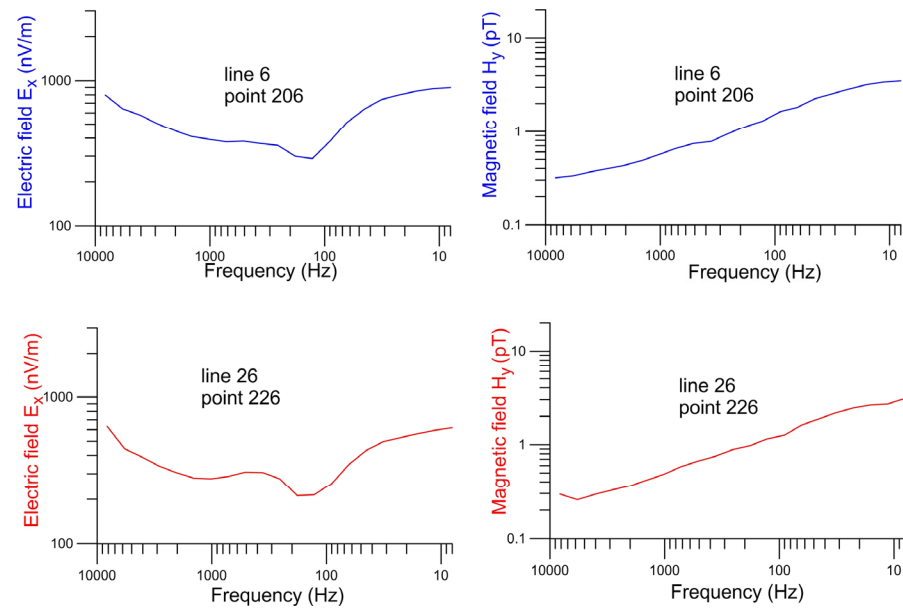
Figure 8. Electromagnetic field curves from the controlled-source audiomagnetotelluric measurement point.

According to geological observations (Figure 9), the first member (T_1f^1) of the Feixianguan Formation consists of greenish-gray lithic feldspathic sandstone, ranging in grain size from coarse to fine, with a thickness varying between 40 cm and 2 m. As one moves upwards, the lithology changes to purplish-red medium-bedded lithic feldspathic sandstone interspersed with layers of purplish-red siltstone (Figure 9a). These sandstones frequently include clasts of purplish-red mudstone and occasional calcareous nodules, while the siltstones sometimes contain small calcite crystals.
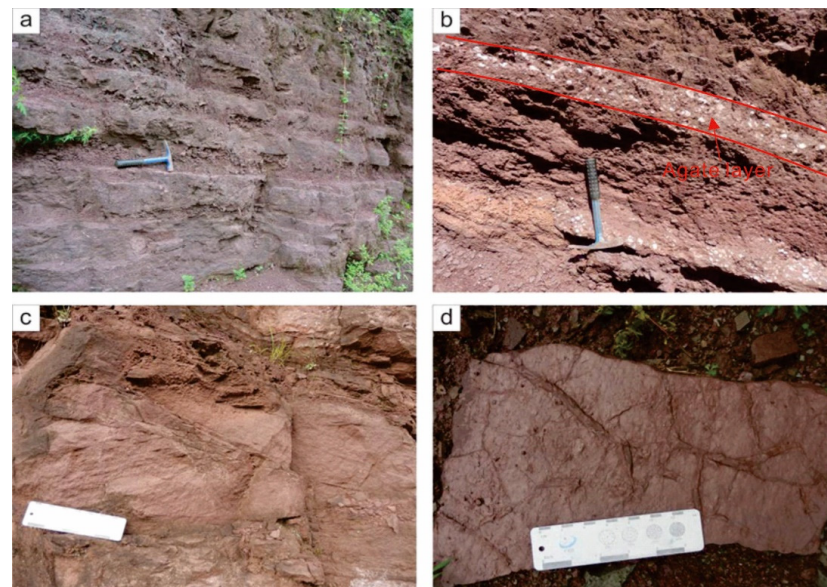

Figure 9. Characteristics of the agate-rich strata of the Feixianguan Formation. Locations of these samples are shown in Figure 2. (**a**) Interbedded sand-mudstone of the first member of the Feixianguan Formation; (**b**) agate conglomerate layer of the second member of the Feixianguan Formation; (**c**) wedge-shaped cross-bedding in the second member of the Feixianguan Formation; (**d**) mudcracks in the third member of the Feixianguan Formation.

The second member (T_1f^2) of the Feixianguan Formation is composed of purplish-red medium-bedded lithic feldspathic sandstone interlayered with purplish-red agate-bearing

lithic feldspathic sandstone, siltstone, or mudstone (Figure 9b). This section is notable for its abundant agate clasts within the sandstone, which exhibits parallel bedding, tabular cross-bedding, and wedge-shaped cross-bedding (Figure 9c).

Vertical electrical sounding (Figure 10) offers high-resolution insights into the subsurface. We used the IP12win software from Moscow State University for the interpretation. The RMS error of point 01 and point 02 is, respectively, 1.2 and 1.6. It showed good data fitting in Figure 11. The results reveal a near-surface low-resistivity layer corresponding to water-rich sandstone, overlying the higher-resistivity gravel-bearing sandstone of the Feixianguan Formation. Beneath this, the sequence transitions to the Xuanwei Formation mudstone and bedrock. Notably, from VES 1 to VES 2, the burial depth of the agate layer progressively decreases.
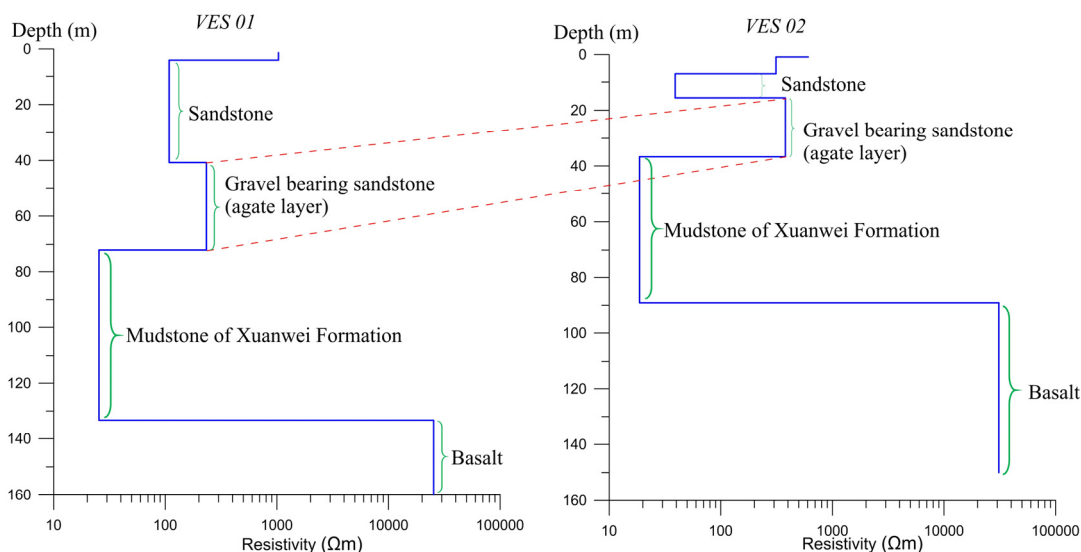

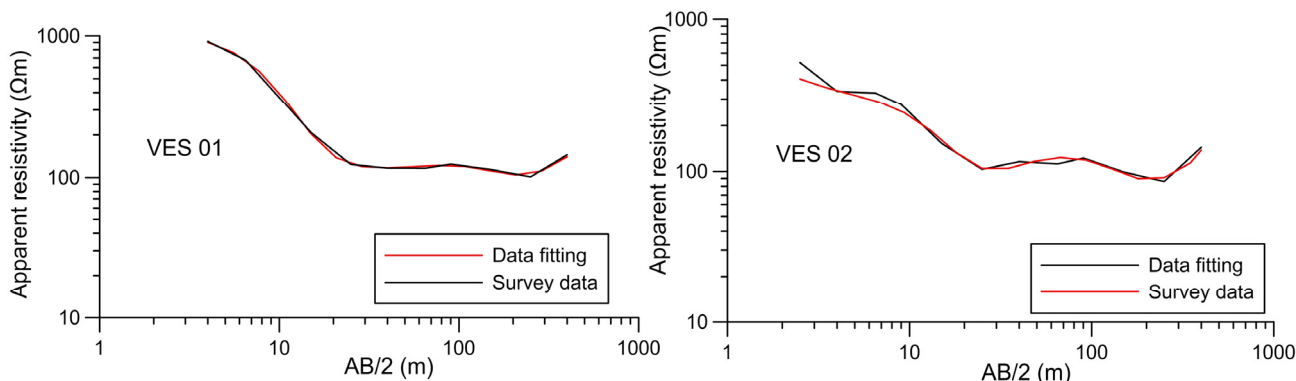**Figure 10.** Inversion results of the vertical electrical sounding points.

Figure 11. Data fitting for vertical electrical sounding.

4.4. Practicality of Integrated Geological and Geophysical Measurements in Agate Exploration

The formation of Nanhong agate in the Liangshan region of Sichuan, China, is primarily influenced by volcanic and sedimentary processes. Late Permian tectonic stresses, mainly manifesting as east–west extensional forces, resulted in the development of north–south trending extensional faults, which triggered extensive volcanic activity. These faults served as conduits for the extrusion and shallow intrusion of basaltic magma and subsequently facilitated the deposition of Nanhong agate through the filling of early volcanic rock cavities by post-volcanism hydrothermal fluids. Additionally, the transformation of primary agate through weathering, erosion, transportation, and diagenesis

contributes to the formation of agate deposits. Sedimentary processes also play a crucial role in this formation.

Our exploration of this distinctive agate-type quartz mineral commenced with geological surveys. By analyzing the unique sedimentary environment and petrological characteristics of the exploration area, we identified geological formations and rock compositions. These foundational data facilitated the rapid delineation of potential mineralized sedimentary strata. Our findings revealed that agate deposits predominantly occur as stratiform or stratiform-like bodies within sedimentary rocks, often appearing as conglomerates or pebbly sandstones, classified as secondary sedimentary deposits. The second conglomerate layer of the Feixianguan Formation is the primary ore-bearing horizon for agate. It exhibits a gentle dip ranging from 5° to 12°, aligning closely with the terrain due to its mild inclination. The grain size is predominantly coarse, consisting mainly of purplish-red fine–medium-grained sandstone interbedded with purplish-red mudstone containing agate. Agate pebbles are commonly found within the sandstone, indicating significant sedimentary hydrodynamics during deposition. Sedimentary structures such as parallel bedding, tabular cross-bedding, and wedge cross-bedding are highly developed, reflecting the strong sedimentary hydrodynamics of the Feixianguan Formation's second conglomerate layer. This layer's ore formation is primarily attributed to an earlier formed agate layer of the Emeishan basaltic formation during the late Permian, which underwent weathering, erosion, transportation, and re-deposition, culminating in the current conglomerate agate layer of the second member of the Feixianguan Formation. The sedimentary environment is predominantly characterized by alluvial fan or deltaic facies. The magmatic rocks in the mining area mainly belong to the Emeishan basaltic group. While ore-controlling structures are not prominently visible and alteration is minimal, the agate primarily exhibits a single-layer structure with colors mainly in shades of cherry red, and they exhibit ice-floating patterns (Figure 3).

Upon delineating the preliminary agate deposit zones through basic field geological surveys, we utilized physical property measurements for geophysical interpretation. High-precision magnetic surveys were conducted to identify potential agate-bearing areas. The CSAMT method was employed to probe deep electrical structure, thereby determining the thickness of the ore-bearing strata and the depth to bedrock. Further precision in determining the depth and thickness of the agate layer was achieved through vertical electrical sounding. Table 2 presents the comparison results between CSAMT, resistivity sounding, and physical property measurements. As shown in the table, the resistivity ranges of geological units measured by various geophysical methods are generally consistent with those obtained from physical property measurements.

Table 2. Comparison of survey results of geophysical methods and resistivity measurements for different geological units.

	Result of CSAMT	Result of Resistivity Sounding	Resistivity Measurements
Gravel bearing agate and conglomerate	100–400 Ωm	200–400 Ωm	382.8 Ωm
Sandstone	100–400 Ωm	20–100 Ωm	141.66 Ωm
Mudstone	10–100 Ωm	20–30 Ωm	/
Basalt	>400 Ωm	>20,000 Ωm	1892.01 Ωm

Previous studies have recognized the shallow burial depth and non-polarizing characteristics of agate, employing ground-penetrating radar for prospecting. Measurements were taken at several study test sites with respect to the subsurface geology of weathered melaphyre and pyroclastic deposits using a GPR system (ProEx) [26]. However, no precedent exists for agate exploration using the combination of geological and electrical methods employed in this study. Therefore, our study integrates geological surveys with

high-precision magnetic surveys, CSAMT, and vertical electrical sounding to construct an agate ore prediction map (Figure 12). The predictive map was constructed using the stratigraphic sequence obtained from geological surveys, incorporating the medium magnetic anomaly of the agate gravel layer and the resistivity parameter values measured for various geological units based on their physical properties, as shown in Table 2.
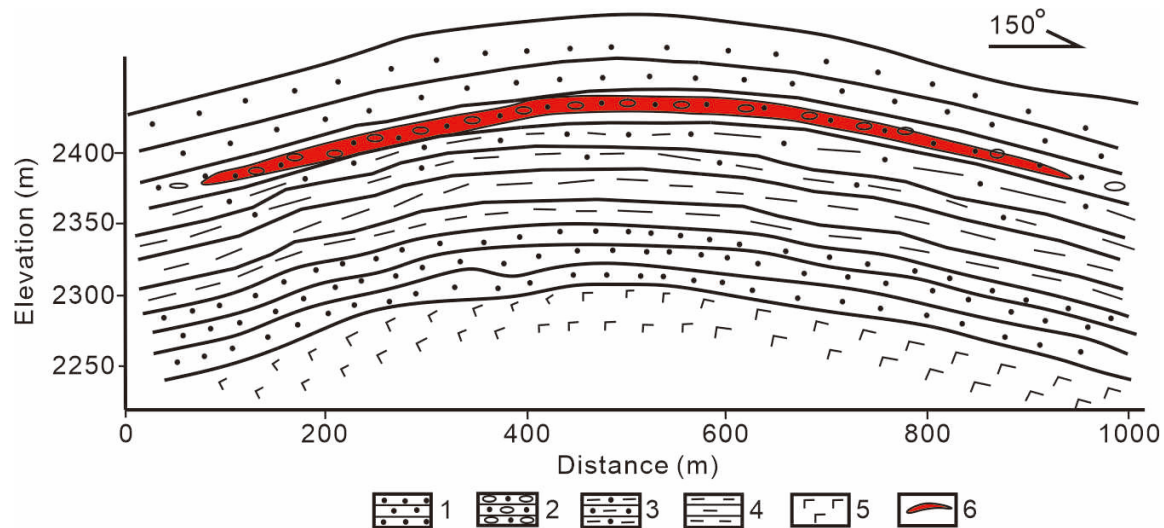

Figure 12. Predicted mineral body map of the agate deposit in the exploration area. 1—Sandstone; 2—conglomeratic sandstone; 3—silty sandstone; 4—mudstone; 5—basalt; 6—agate. Location of this predicted mineral is shown in Figure 2.

Our extensive survey indicates that the surface is largely dominated by sandstone, with agate deposits found within the conglomerate layer of the second member of the Feixianguan Formation, which comprises pebbly sandstones. This layer is underlain by the mudstones of the Xuanwei Formation and sits atop the Emeishan basalt bedrock. According to the ore prediction map, agate deposits are identifiable by targeting high-resistivity and magnetically active conglomerate layers within the second member of the Feixianguan Formation. Consequently, the applied methods and techniques for exploring agate-bearing horizons have proven effective. This study confirms that geological surveys, physical property measurements, and geophysical methods, particularly high-precision magnetic surveys and CSAMT, are powerful tools for chalcedony mineral exploration.

5. Conclusions

In this study, geological investigations were undertaken to identify the ore-bearing strata, sedimentary environments, and petrological characteristics of agate deposits in the Liangshan region of Sichuan, China. This strategy significantly narrowed the exploration area. Advanced geophysical exploration methods, including high-precision magnetic surveys, CSAMT techniques, and vertical electrical sounding, were then applied to enhance differentiation capabilities. These techniques successfully identified the agate-bearing strata, the low-resistivity mudstones of the Xuanwei Formation, and the underlying bedrock, leading to the creation of a comprehensive mineral prediction map that details the distribution of ore-bearing agate layers.

Our results indicate that the agate deposits are primarily located within the conglomeratic sandstone layer of the second member of the Triassic Feixianguan Formation, characterized by relatively high resistivity and a thickness of approximately 40 m. Beneath this layer lies the low-resistivity mudstones of the Xuanwei Formation, underlain by the highly magnetic Permian Emeishan basalt.

This research provides a solid scientific basis for the precise identification and evaluation of Nanhong agate deposits and introduces new perspectives and methodologies

for exploring similar quartz mineral deposits. We believe that the insights gained from this study will significantly contribute to the responsible exploitation and utilization of Nanhong agate resources. Additionally, the methods and findings presented are expected to serve as a crucial reference for geophysical exploration efforts targeting quartz mineral deposits worldwide.

Author Contributions: Conceptualization, methodology, soft, formal analysis, writing: S.G. and J.Y.; geological investigation: S.Y. and K.Z.; geophysical investigation, geophysical data methodology and analysis: S.G.; Project manager: Y.L.; Document editing: J.Y. and M.W. All authors have read and agreed to the published version of the manuscript.

Data Availability Statement: Data are available to request from the China Geological Survey. https://geocloud.cgs.gov.cn/.

Conflicts of Interest: The authors declare no conflicts of interest.

References

1. Huang, Y.F.; Hua, D.J.; Jia, Q. Characteristics and prospecting prospects of agate deposits in the Lomoyida area of Sichuan Province. *China Sci. Technol. Inf.* **2022**, *8*, 73–75.
2. Zhou, Y.; Liu, Z.; Zhao, Z.; Guo, Y. Quantitative study on colour and spectral characteristics of Beihong agate. *Minerals* **2022**, *12*, 677. [CrossRef]
3. What Is South Red Agate in Chinese Jewelry? 2023. Available online: https://www.chinese-showcase.com/blogs/jewelry/what-is-south-red-agate-in-chinese-jewelry (accessed on 2 August 2023).
4. Tang, F.; Lin, F.; Jin, C.; Deng, G.; Zhao, H.; Tie, Y.; Yu, Q.; Ren, S.; Ren, G. Practical geological technologies facilitating poverty alleviation in Wumeng Mountain area. *China Geol.* **2020**, *3*, 504–508. [CrossRef]
5. Chen, S.Y.; Wang, S.Q.; He, X.M.; Luo, B.; Zhou, C.J.; Shi, X.P. Preliminary study of the characteristics and genesis of the Nanhong agate deposit in Liangshan, Sichuan, China. *Jewel. Technol.* **2015**, *1*, 196–199.
6. Jing, H.X.; He, Y.G.; Luo, B.; Li, J.J.; Liu, W.; Wang, N. Characteristics of occurrence and genesis of Nanhong agate deposit in Waxi area, Meigu county, Sichuan province. *Contrib. Geol. Miner. Resour. Res.* **2023**, *38*, 326–330.
7. Baranwal, V.C.; Rønning, J.S.; Larsen, B.E.; Su, Y.; Zhang, B.; Liu, Y.; Ren, X.; Gautneb, H.; Gellein, J. A case history of graphite exploration in north Norway integrating various geophysical surveys. *Minerals* **2024**, *14*, 266. [CrossRef]
8. Gong, S.; Yang, Y.; Lin, P.; Wu, W.; Zheng, C.; Shi, F.; Wu, X.; Weng, A.; Zhang, G.; Gu, G.; et al. Three-dimensional electrical exploration methods for the mapping of polymetallic targets in Gansu Province, China. *Geophys. Prospect.* **2019**, *67*, 1929–1947. [CrossRef]
9. Gong, S.P.; Yang, Y.B.; Zhang, G.Z.; Lin, P.R.; Wu, W.L.; Zhen, C.J.; Shi, F.S. Experimental study on 3D time-domain electromagnetic exploration in Huaniushan Pd-Zn deposit. *Sci. Technol. Eng.* **2018**, *18*, 16–24.
10. Gong, S.P.; Lu, G.F.; Xi, M.J.; Ma, S.M.; Su, W.L. The application of integrated geophysical and geochemical methods to the prospecting of copper polymetallic deposits in the arid desert area. *Geophys. Geochem. Explor.* **2021**, *45*, 1–10.
11. Yang, J.; Zhao, L.; Shen, Y.; Shi, K. Application research of controlled source acoustic magnetotelluric in the location forecasting of buried orebodies. *Geol. Sci. Technol. Inf.* **2000**, *19*, 107–112.
12. Zhang, G.; Li, R. The test result of the controlled audio-frequency magnetotelluric method in the prospecting for deep ore deposits. *Geophys. Geochem. Explor.* **2010**, *34*, 66–70.
13. Huang, H.; Cawood, P.A.; Hou, M.; Yang, J.; Ni, S.; Du, Y.; Yan, Z.; Wang, J. Silicic ash beds bracket Emeishan Large Igneous province to <1 m.y. at ~260 Ma. *Lithos* **2016**, *264*, 17–27.
14. Tschirhart, V.; Morris, B. Physical Rock Property Constraints and Regional Geophysical Interpretations of the Northeast Thelon Basin, Nunavut. 2017. Available online: https://www.academia.edu/70174978/Physical_Rock_Property_Constraints_and_Regional_Geophysical_Interpretations_of_the_Northeast_Thelon_Basin_Nunavut (accessed on 25 April 2024).
15. Kozhevnikov, N.O.; Kamnev, Y.K.; Kazansky, A.Y. Error analysis of frequency-dependent magnetic susceptibility measurements: Magnetic viscosity studies with the Bartington MS2 system. *Russ. Geol. Geophys.* **2014**, *55*, 508–514. [CrossRef]
16. Li, L.; Guo, Y.; Chen, X. Development of RP-1 type rock and ore electrical measurement system. *Geophys. Geochem. Explor.* **2013**, *3*, 529–532.
17. Hallimond, A.F.; Herroun, E.F. Laboratory determinations of the magnetic properties of certain igneous rocks. *Proc. R. Soc. London. Ser. A Contain. Pap. A Math. Phys. Character* **1933**, *141*, 302–314.

18. Legowo, B.; Irfan, N.M.; Suryanto, W.; Purnama, B. Study comparison physical properties and minerals analysis of rock magnetic in Lawu Volcanic Complex. *J. Phys. Conf. Ser.* **2023**, *2498*, 012033. [CrossRef]

19. Essaa, K.S.; Nadyb, A.G.; Mostafab, M.; Elhussein, M.S. Implementation of potential field data to depict the structural lineaments of the Sinai Peninsula, Egypt. *J. Afr. Earth Sci.* **2018**, *147*, 43–53. [CrossRef]

20. Biswas, A.; Rao, K. Interpretation of magnetic anomalies over 2D fault and Sheet-Type mineralized structures using very fast simulated annealing global optimization: An understanding of uncertainty and geological implications. *Lithosphere* **2021**, *2021*, 2964057. [CrossRef]

21. Essa, K.S.; Elhussein, M. Magnetic interpretation utilizing a new inverse algorithm for assessing the parameters of buried inclined dike-like geological Structure. *Acta Geophys.* **2019**, *67*, 533–544. [CrossRef]

22. Petronis, M.; Valenta, J.; Rapprich, V.; Lindline, J.; Heizler, M.; Vries, B.; Shields, S.; Balek, J.; Fojtíková, L.; Tábořík, P. Emplacement history of the Miocene Zebín Tuff Cone (Czech Republic) revealed from ground geophysics, anisotropy of magnetic susceptibility, paleomagnetic, and 40Ar/39Ar geochronology data. *Geochem. Geophys. Geosystems* **2018**, *19*, 3764–3792. [CrossRef]

23. Amaral, P.A.C.; Borges, W.R.; Toledo, C.L.B.; Silva, A.M.; Godoy, H.V.; Santos, M.H. Electrical prospecting of gold mineralization in exhalites of the Digo-Digo VMS occurrence, central Brazil. *Minerals* **2023**, *13*, 1483. [CrossRef]

24. Nazari, S.; Rochlitz, R.; Günther, T. Optimizing semi-airborne electromagnetic survey design for mineral exploration. *Minerals* **2023**, *13*, 796. [CrossRef]

25. Wu, Y.; Xie, H.; Ji, Y.; Zhao, P.; Wang, Y. The potential of the horizontal component TEM data in the detection of polarizable mineral: Synthetic cases. *Minerals* **2023**, *13*, 523. [CrossRef]

26. Mierczak, M.; Karczewski, J. Location of agate geodes in Permian deposits of Simota gully using the GPR. *Acta Geophys.* **2021**, *69*, 655–664. [CrossRef]

27. Sandberg, S.K.; Hohmann, G.W. Controlled-Source Audiomagnetotellurics in Geothermal Exploration. Topical Report. *Geophysics* **1980**, *47*, 100–116. [CrossRef]

28. Wang, J.; Wang, M.; Liu, W.; Lin, P. The full-field apparent resistivity of CSAMT defined by the magnetic field y-component and an application to a geological survey in the Xiong'an New Area, China. *Bull. Geophys. Oceanogr.* **2022**, *63*, 311–324.

29. Atya, M.; Meneisy, A.M.; Bedair, S. Integration of electrical resistivity and time-domain electromagnetic to investigate the subsurface stratigraphic conditions at Assiut Power Plant, Assiut, Egypt. *J. Astron. Geophysics.* **2020**, *9*, 471–482. [CrossRef]

30. Hamzah, U.; Samsudin, A.R.; Malim, E.P. Ground water investigation in Kuala Selangor using vertical electrical sounding (VES) surveys. *Environ. Geol.* **2007**, *51*, 1349–1359. [CrossRef]

31. Shen, M.; Lu, Z.; He, X. Mineralogical and geochemical characteristics of banded agates from Placer deposits: Implications for agate genesis. *Acs Omega* **2022**, *7*, 23858–23864. [CrossRef]

32. Yan, S.; Zhao, C.; Qin, Y.; Bai, X. The geological characteristics and mineralization regularities of the Nanhong agate deposit in Zhaojue-Meigu area. In Proceedings of the 1st China Exploration GeoScience Conference (CEGC), Hefei, China, 15–20 September 2021.

33. Macinnes, S.; Raymoned, M. *SCSINV Documentation Zonge Data Processing Smooth-Model CSAMT Inversion Version 2.20*; Zonge Engineering and Research Organization, Inc.: Tucson, AZ, USA, 2006.

34. *DZ/T 0280-2015*; Technical Regulation for Controlled Source Audio Magnetelluric Method. Geological Press: Beijing, China, 2015.